Electronic Supplementary Information

A Universal Strategy for Defects and Interface Management Enables Highly Efficient and Stable Inverted Perovskite Solar Cells

Wenwu Zhou, Yunhe Cai, Shuo Wan, Yi Li, Xiaoying Xiong, Fangcong Zhang, Huiting Fu and Qingdong Zheng*

W. Zhou, Y. Cai, S. Wan, Y. Li, X. Xiong, F. Zhang, Prof. H. Fu, Prof. Q. Zheng
State Key Laboratory of Coordination Chemistry, College of Engineering and Applied Sciences, Nanjing University, Nanjing 210023, China
*E-mail: zhengqd@nju.edu.cn

Materials

Indium tin oxide (ITO) glass substrates were purchased from SuZhou ShangYang Solar Technology Co., Ltd (12 Ω per square). The solvents and reagents were used without additional purification. N,N-dimethylformamide (DMF, 99.8%), dimethyl sulfoxide (DMSO, 99.7%), anisole (OMe, 99%) and isopropanol (IPA, 99.5%) were purchased from J&K Scientific Ltd. Ethanol (EtOH, 99.5%), chlorobenzene (CB, 99.8%), bathocuproine (BCP, 96%) and rubidium iodide (RbI, 99.9%) were purchased from Merck Chemicals (Shanghai) Co., Ltd. Lead (II) iodide (PbI_2, 99.999%), cesium bromine (CsBr, 99.9%), cesium iodide (CsI, 99.999%), methylammonium iodide (MAI, 99.9%), methylammonium chloride (MACl, 99.9%), Lead (II) bromide ($PbBr_2$, 99.99%) and [6,6]-phenyl-C61-butyric acid methyl ester ($PC_{61}BM$, 99%) were purchased from Xi'an Yuri Solar Co., Ltd. Formamidinium iodide (FAI, 99.99%) was purchased from Advanced Election Technology Co., Ltd. [2-(3,6-Dimethoxy-9H-carbazol-9-yl)ethyl] phosphonic acid (MeO-2PACz, >98%) was purchased from the TCI (Shanghai) Development Co., Ltd. 2-Phenylethylamine hydrobromide (PEABr, 99.5%) was purchased from Shanghai ACMEC Biochemical Technology Co., Ltd. 5-Amino-1,3,4-thiadiazole-2-thiol (5ATT, 97%) was purchased from the Shanghai Bide Pharmatech Co., Ltd.

Device fabrication

The ITO glass substrates were sequentially washed in ultrasonic bath for 20 min using a mixed solution of deionized water and detergent, deionized water, ethanol as well as

isopropanol. The cleaned ITO glass substrates were dried in an oven at 70 ℃ until the residual solvent was completely evaporated. Then, the ITO glass substrates were subjected to ultraviolet–ozone cleaning for 25 min for fabricating perovskite solar cells (ITO/MeO-2PACz/perovskite/$PC_{61}BM$/BCP/Ag. The MeO-2PACz (0.5 mg/mL in ETOH) was spin-coated on the ITO glass substrates at 3000 rpm for 30 s and then annealed at 100 ℃ for 10 min. After cooling down to room temperature, the perovskite films were prepared on the MeO-2PACz layer.

For the $MAPbI_3$ perovskite (single cation at A-site), 468 mg of PbI_2 and 159 mg of MAI were dissolved in the 640 μL DMF and 73 μL DMSO mixed solution and stirred at 50 ℃ for 2 hours. The prepared perovskite precursor solution was dropped on the MeO-2PACz layer, and spin-coated at 4000 rpm for 25s. The 150 μL CB was poured on the perovskite at the 17s quickly and then annealed at 100 ℃ for 10 min to acquire the perovskite films.

For the $FA_{0.85}Cs_{0.15}Pb(I_{0.95}Br_{0.05})_3$ perovskite (double cations at A-site), the perovskite precursor solution (1.5 M) was prepared by mixing FAI, PbI_2 and CsBr in 1 mL of DMF: DMSO mixed solvents (4: 1, v: v) in reference of the stoichiometric ratio of $FA_{0.85}Cs_{0.15}Pb(I_{0.95}Br_{0.05})_3$. The perovskite films were obtained by one-step spin-coating the precursor on MeO-2PACz layer at 6000 rpm for 60 s, 150 μL of CB was quickly poured on the perovskite to extract the mixed solvents at the beginning of 15 s, and then annealed at 100 ℃ for 30 min.

For the $FA_{0.85}MA_{0.1}Cs_{0.05}PbI_3$ perovskite (triple cations at A-site), 1.5 M perovskite precursor solution was obtained by dissolving FAI, PbI_2 (10% of excess), CsI and MAI in 1 mL of DMF: DMSO (4: 1, v: v) mixed solvents according to the stoichiometric ratio of $FA_{0.85}Cs_{0.05}MA_{0.1}PbI_3$. In order to obtain better crystallization, 12.5 mol% of MACl was added into the perovskite precursor. The precursor was dropped on the Ph-4PACz layer, and spin-coating at 1000 rpm for 10 s and 5000 rpm for 40 s, respectively (HTL of Ph-4PACz was used for this type of PSCs). Before the end of 5 s, 200 μL of CB was introduced into the perovskite to obtain as-prepared perovskite films and then annealed at 100 ℃ for 30 min.

For the $FA_{0.85}MA_{0.05}Cs_{0.05}Rb_{0.05}Pb(I_{0.95}Br_{0.05})_3$ perovskite (quadruple cations at A-site), the stoichiometric ratio (1.5 M) of PbI_2, FAI, CsI, $PbBr_2$, MABr and RbI were dissolved in 1 mL of DMF: DMSO (4: 1, v: v) mixed solvents to obtain the perovskite precursor. The perovskite precursor was spin-coated on the MeO-2PACz layer at 1000 rpm for 10 s and 3000 rpm for 40 s. During spin-coating process, 150 μL of CB was dropped on the perovskite at 25 s, prior to the end of the second procedure, and then annealed at 100 ℃ for 10 min.

For the $FA_{0.8}MA_{0.15}Cs_{0.05}Pb(I_{0.75}Br_{0.25})_3$ perovskite (1.68 eV bandgap), According to stoichiometric ratio (1.3 M) of $FA_{0.8}MA_{0.15}Cs_{0.05}Pb(I_{0.75}Br_{0.25})_3$, the PbI_2, FAI, CsI, $PbBr_2$ and

MABr were dissolved in the 1 mL of mixed solvents of DMF: DMSO (4: 1, v: v). The obtained perovskite precursor solution was dropped on MeO-2PACz layer and spin-coated by a two-step processes (1000 rpm for 8 s and 6000 rpm for 30 s). At the end of 8 s, 300 μL of anisole was quickly poured on the perovskite and then the as-prepared perovskite films were annealed at 100 ℃ for 15 min.

For the $FA_{0.8}Cs_{0.2}Pb(I_{0.6}Br_{0.4})_3$ perovskite (1.77 eV bandgap), based on the stoichiometric ratio (1.2 M) of $FA_{0.8}Cs_{0.2}Pb(I_{0.6}Br_{0.4})$, the PbI_2, FAI, CsI and $PbBr_2$ were dissolved in the 1 mL of mixed solvents of DMF: DMSO (4: 1, v: v) and stirred at 50 ℃ for 2 h. The perovskite precursor was spin-coated on the MeO-2PACz layer by a two-step spin-coating procedure (1000 rpm for 10 s and 5000 rpm for 30 s). 200 μl of CB was dropped on the perovskite at 7 s during the second spin-coating step and then annealed at 100 ℃ for 20 min.

For the $FA_{0.8}MA_{0.1}Cs_{0.1}Pb(I_{0.5}Br_{0.5})_3$ perovskite (1.82 eV bandgap), in reference of the stoichiometric ratio (1M) of $FA_{0.8}MA_{0.1}Cs_{0.1}Pb(I_{0.5}Br_{0.5})_3$, the PbI_2, FAI, CsI, $PbBr_2$ and MAI were dissolved in the 1 mL mixed solvents of DMF: DMSO (4: 1, v: v). The perovskite films were fabricated on the MeO-2PACz layer by spin-coating at 1000 rpm for 10 s and 4000 rpm for 40 s. At 25 s of the second step, 180 μl of CB was dropped, and then quickly transfer the as-prepared perovskite films to the heating stage to anneal at 100 ℃ within 10 min.

Subsequently, the mixed passivating agents of PEABr+5ATT (1 mg of PEABr and 1.5 mg of 5ATT) were dissolved in 1 mL of IPA and then was spin-coated on the cooled perovskite films at 5000 rpm for 30 s, and followed by annealing at 100 ℃ for 10 min. After cooling down to room temperature, the $PC_{61}BM$ solution (20 mg/mL, CB) was spin-coated on the PEABr+5ATT layer at 2000 rpm for 30 s and annealed at 70 ℃ for 10 min. The BCP solution (0.5 mg/mL, IPA) was spin-coated on the $PC_{61}BM$ layer at 4000 rpm for 30 s, and annealed at 70 ℃ for 10 min. Finally, the devices were finished by evaporating 100 nm of Ag in a vacuum chamber of $<1x10^{-4}$ Pa.

Perovskite film characterizations

The ^1H nuclear magnetic resonance spectra (^1H NMR) of the passivating agents dissolved in DMSO-d_6 solvent were measured by Bruker Avance III 400 MHz spectrometer. The X-ray photoelectron spectroscopy (XPS) spectra of the control, PEABr- and PEABr+5ATT- treated perovskite films were collected by the Thermo Scientific Al K-Alpha XPS system with energy steps of 0.1 eV. The X-ray diffraction (XRD) patterns were taken by a Bruker D8 AVANTAGE diffractometer with Cu Kα radiation (1.54 Å). The grazing incident wide-angle X-ray scattering (GIWAXS) results were collected by the XEUSS SAXS/WAXS

equipment at the Fujian Science & Technology Innovation Laboratory for Optoelectronic Information of China, and the incident angle of the X-ray beam was set to 0.5°. The surface morphology was obtained by scanning electron microscopy (SEM, HITACHI SU8010) with a working voltage of 5 kV. The thicknesses of the perovskite films that coated on the ITO glass substrates were marked by a Bruker Dektak XT profilometer. Atomic force microscopy (AFM) and Kelvin Probe Force Microscopy (KPFM) were performed for the control, PEABr- and PEABr+5ATT-treated perovskite films by Bruker Dimension Icon SPM system. Ultraviolet-visible (UV-vis) absorption spectra were tested by a UV-vis spectrometer (UV-2450) in the range of 300-900 nm. Photoluminescence (PL) measurements were conducted by a HORIBA Nanolog fluorescence spectrometer (excitation wavelength is 485 nm). Time-resolved photoluminescence (TRPL) decay curves were measured using a HORIBA Fluorolog-3 time-correlated single photon counting system (excitation wavelength is 485 nm), and the corresponding carrier lifetimes were fitted by two exponential functions according to the equation (1)[1]. The PL intensity and carrier lifetime mapping images were obtained in a scanning area of 50*50 μm^2 by the ISS Q2 laser confocal microscopy system. The photoluminescence quantum yields (PLQY) of perovskite films with ITO/HTL/perovskite as well as ITO/HTL/perovskite/ETL stacks were measured by an Ocean Optics QEPro spectrometer, with a 405 nm laser inside an integrated sphere (Newport, 70682NS). The internal quasi-Fermi level splitting (QFLS) was calculated according to our previous work.[2]

$$\tau_{ave}=(A_1\tau_1+A_2\tau_2)/(A_1+A_2) \quad (1)$$

τ_{ave} is the carrier lifetime, τ_1 is time constant for fast decay component and τ_2 is time constant for slow decay component. The A_1 and A_2 represent the decay amplitude of the fast and slow decay process, respectively. All of the characterized perovskite is FAMACsRb.

Device characterizations

The *J-V* curves of the perovskite solar cells with a working area of 0.042 cm^2 were tested by a source meter (Keithley 2400) under AM1.5G (100 mW cm^{-2}) illumination in the N_2-filled glovebox. The external quantum efficiency (EQE) spectra were measured by QE-R Solar Cell Spectral Response Measurement System (Enli Technology Co., Ltd., Taiwan) and the light intensity was calibrated with standardized Si solar cell before the measurements. The electrochemical impedance spectroscopy (EIS) and Mott–Schottky were characterized by the

CHI604E electrochemical workstation. The space-charge-limited current (SCLC) method was used to calculate the trap density (N_{trap}) with the ITO/SnO_2/perovskite/$PC_{61}BM$/BCP/Ag structures with and without treatments. According to the Mott Gurney law, the Ohmic region is at low voltage, trap-filled limited region is at intermediate voltage and trap-filled child region is at high voltage, respectively. The N_{trap} can be calculated by the formula[3]:

$$N_{trap} = 2\varepsilon_r\varepsilon_0 V_{TFL}/(ed^2) \quad (2)$$

where ε_r is relative dielectric constant of the perovskite, ε_0 is the vacuum permittivity, d is the thickness of the perovskite film, and V_{TFL} is the trap-filled limit voltage.

Density functional theory (DFT) calculations

The density functional theory (DFT) calculations were performed by the program package of DMol3 and CASTEP, and the generalized-gradient approximation (GGA) with the Perdew-Burke-Emzerhof (PBE) formulation was used. For the ESP calculation, the DMol3 was taken and the corresponding optimization steps were stopped until the total energy converged to 10^{-6} eV/atom. For the defect formation energy calculations, the primitive α-$FAPbI_3$ cell was optimized by allowing to relax to atomic positions and lattice parameters. The optimized α-$FAPbI_3$ cell was used to build the slab with a vacuum layer of 20 Å and the structure was optimized by merely allowing the atomic positions relaxing. The successful calculating results were obtained when the total energy converged to 10^{-5} eV/atom, forces on each unconstrained atom < 0.03 eV/Å, maximal stresses < 0.05 GPa and displacements < 0.001 Å, simultaneously. Moreover, the plane-wave energy cutoff (550 eV) and k-point mesh (3×3×1) were considered. The 5ATT was set on the (001) crystal plane of α-$FAPbI_3$ for calculating the total energy, density of state (DOS) and charge transfer. The defect formation energy (E_f) was calculated by the following equations[4].

$$E_f = E_{defect} + E_a - E_{perfect} \quad (3)$$

Where the E_{defect}, E_a, and $E_{perfect}$ mean that the total energy of defect system, defects (V_I, V_{Pb} or V_{FA}) and perfect system, respectively.

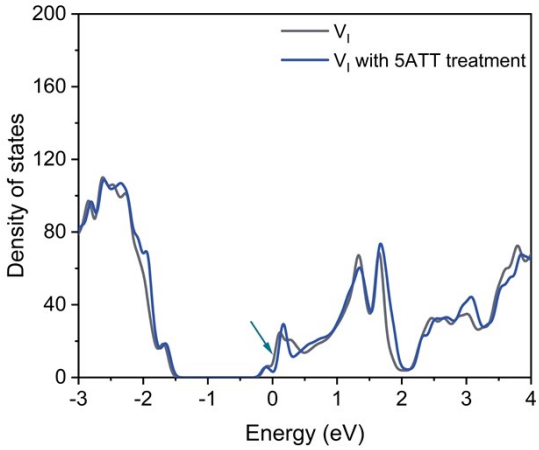

Fig. S1. The DOS of V_I with and without 5ATT treatment.

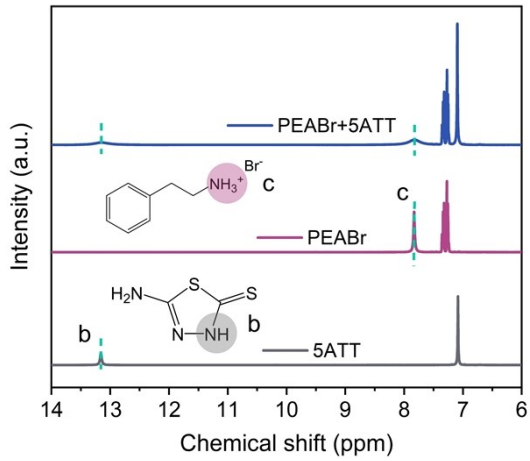

Fig. S2. ^{1}H NMR spectra of 5ATT, PEABr and PEABr+5ATT dissolved in DMSO-d_6.

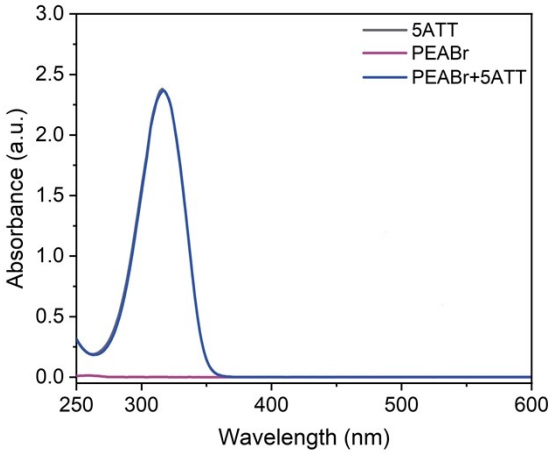

Fig. S3. UV-Vis absorption spectra of 5ATT, PEABr and PEABr+5ATT dissolved in isopropanol.

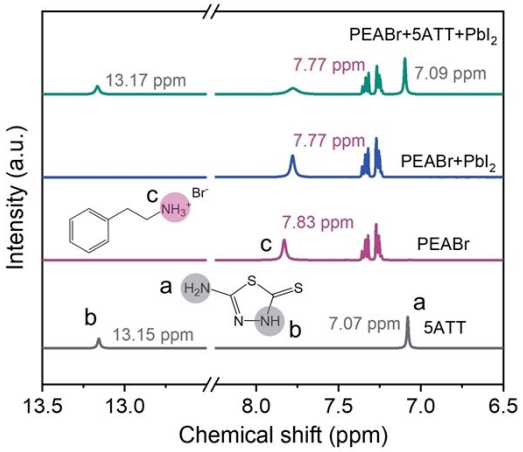

Fig. S4. ^{1}H NMR spectra of PEABr+5ATT+PbI_2 dissolved in DMSO-d6.

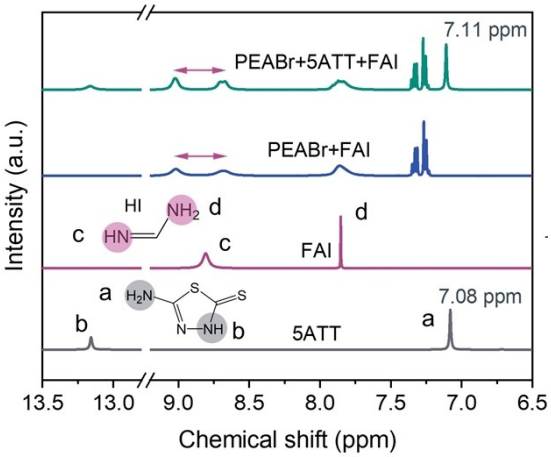

Fig. S5. ^{1}H NMR spectra of PEABr+5ATT+FAI dissolved in DMSO-d6.

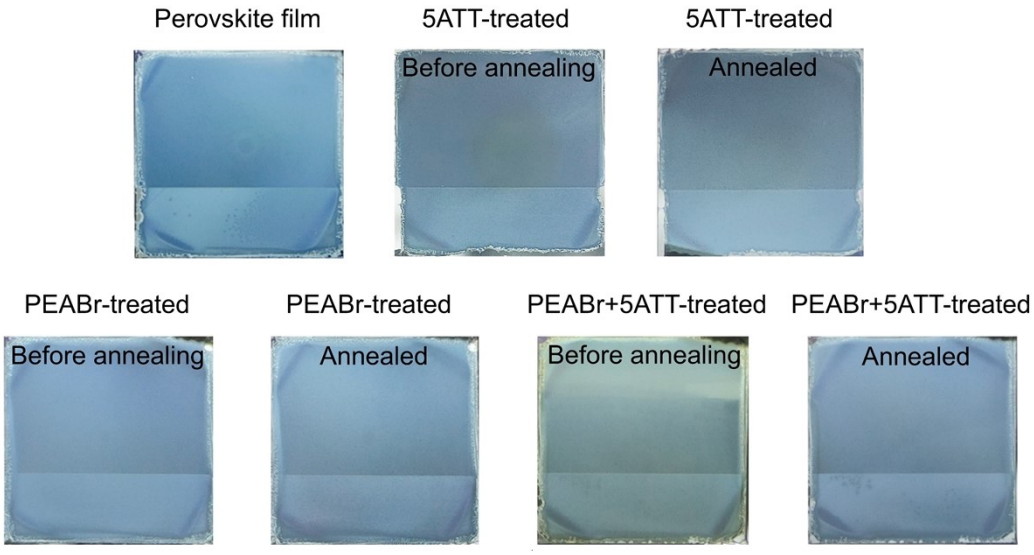

Fig. S6. The color changes of the perovskite films before and after the treatments of 5ATT, PEABr and PEABr+5ATT, respectively.

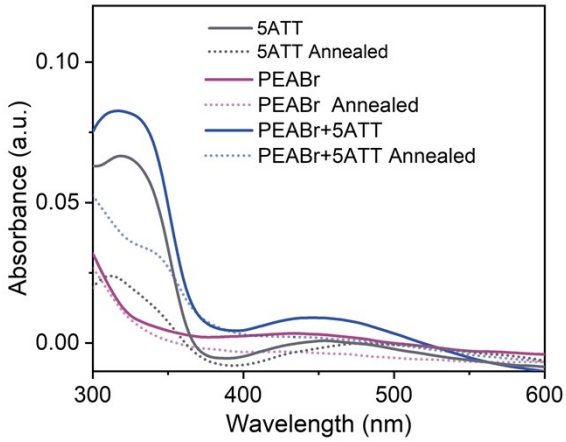

Fig. S7. UV-Vis absorption spectra of 5ATT, PEABr and PEABr+5ATT films with and without annealing at 100 ℃ for 10 minutes.

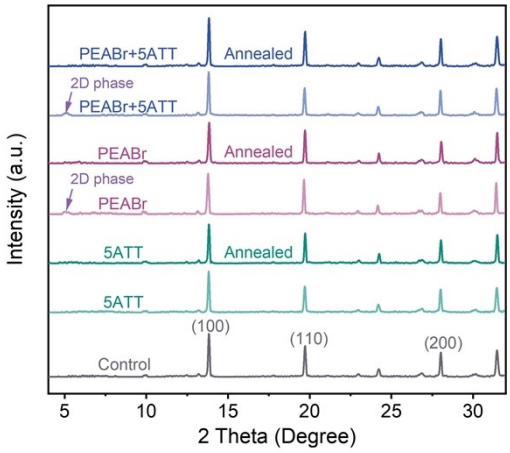

Fig. S8. The XRD patterns of 5ATT-, PEABr- and PEABr+5ATT-treated perovskite films before and after annealing at 100 ℃ for 10 minutes.

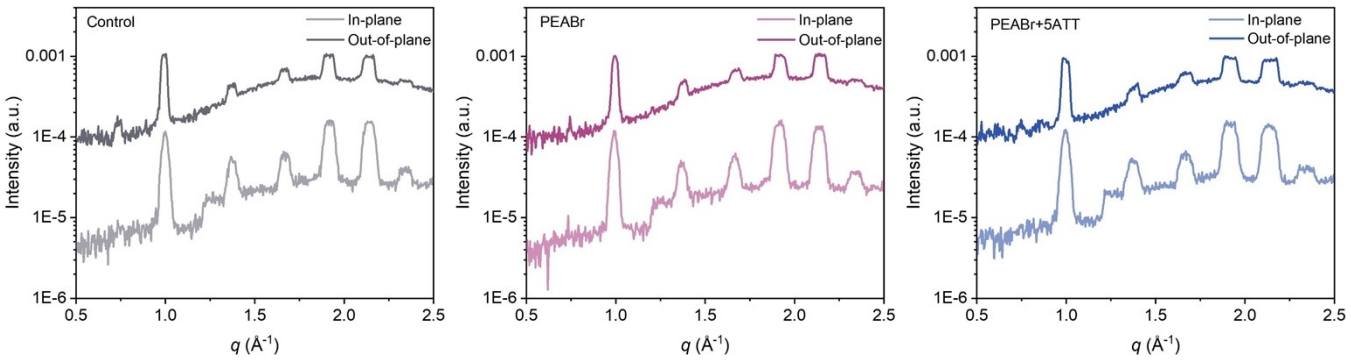

Fig. S9. GIWAXS profiles of out-of-plane direction (q_z) and in-plane direction (q_{xy}) of perovskite films.

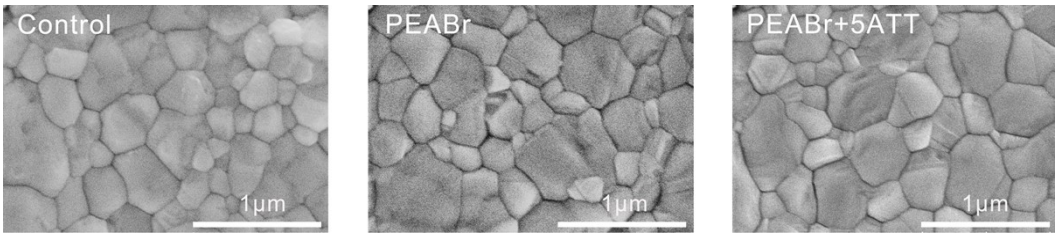

Fig. S10. SEM images of the control, PEABr- and PEABr+5ATT-treated perovskite films.

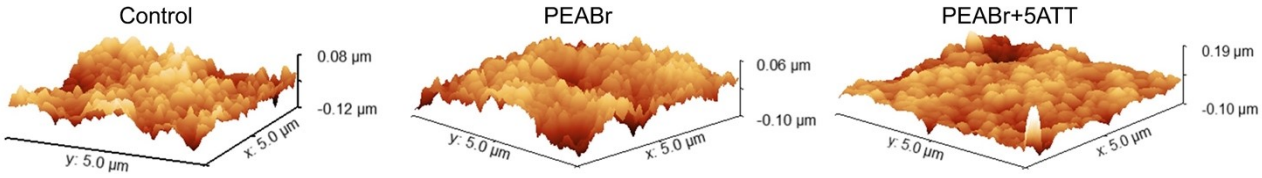

Fig. S11. 3D AFM images of the control, PEABr- and PEABr+5ATT-treated perovskite films.

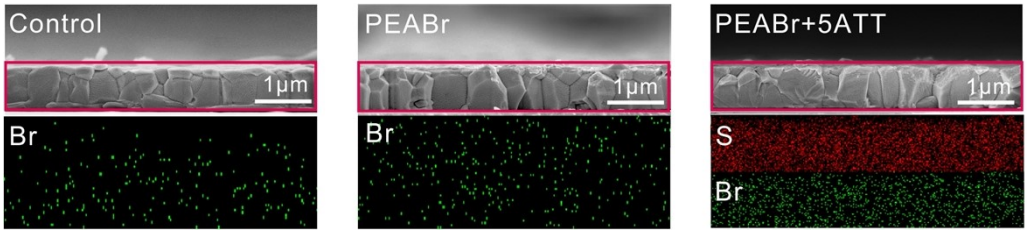

Fig. S12. The cross-sectional SEM images and EDS mappings of the control, PEABr- and PEABr+5ATT-treated perovskite films.

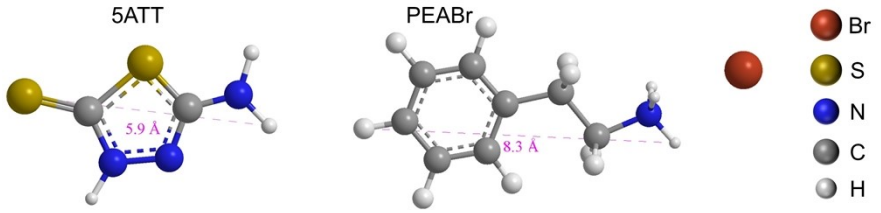

Fig. S13. The molecular sizes of 5ATT and PEABr.

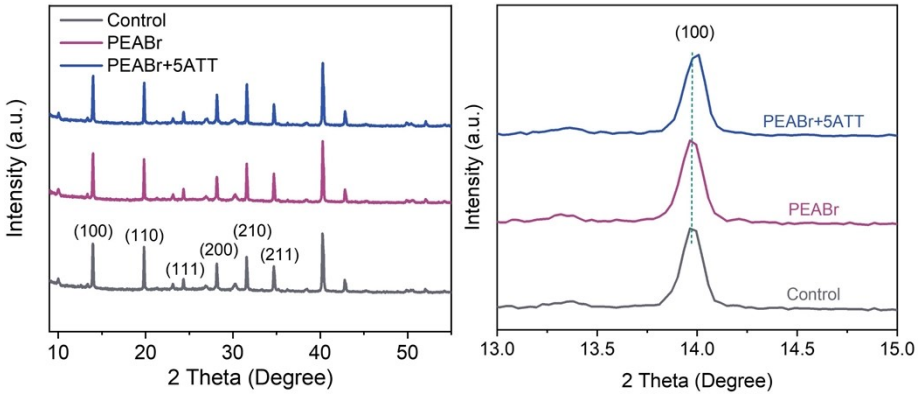

Fig. S14. The XRD patterns and enlarged (100) diffraction peak of the control, PEABr- and PEABr+5ATT-treated perovskite films.

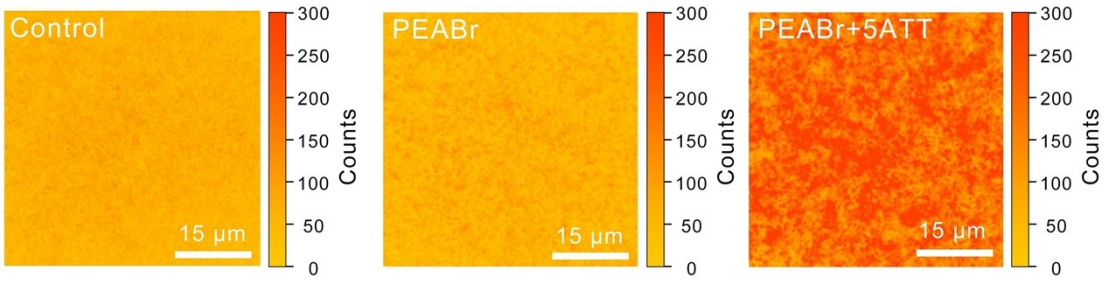

Fig. S15. PL mappings of the control, PEABr- and PEABr+5ATT-treated perovskite films.

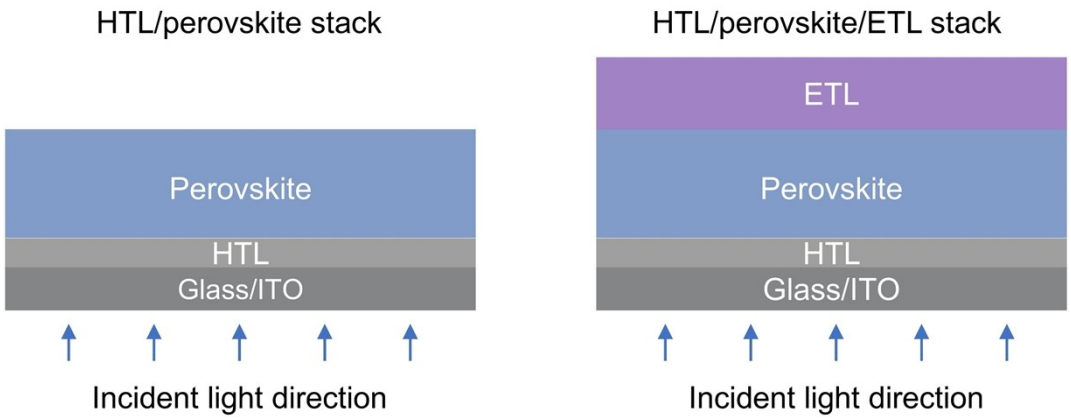

Fig. S16. Two types of stacks for PLQY measurements.

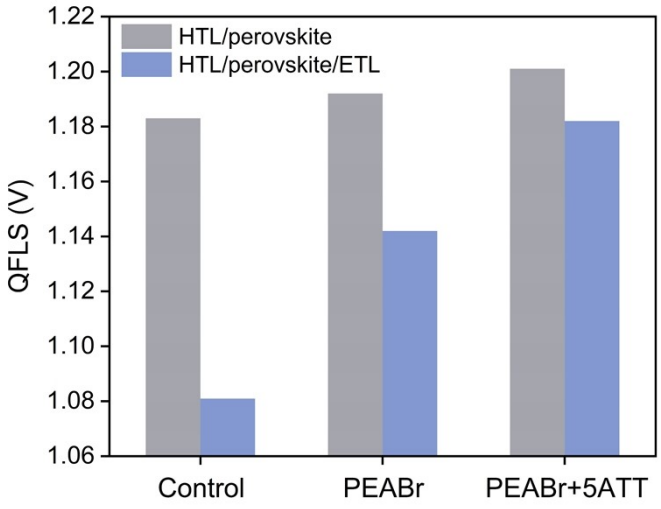

Fig. S17. Calculated QFLS of the HTL/perovskite and HTL/perovskite/ETL stacks based on the PLQY results.

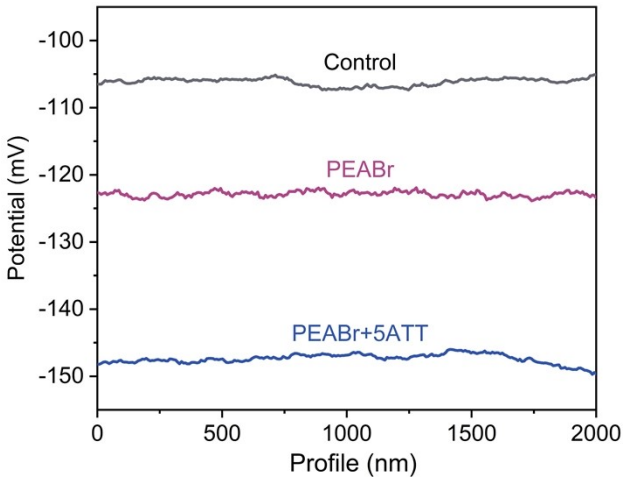

Fig. S18. The mean surface potential of the control, PEABr- and PEABr+5ATT-treated perovskite films.

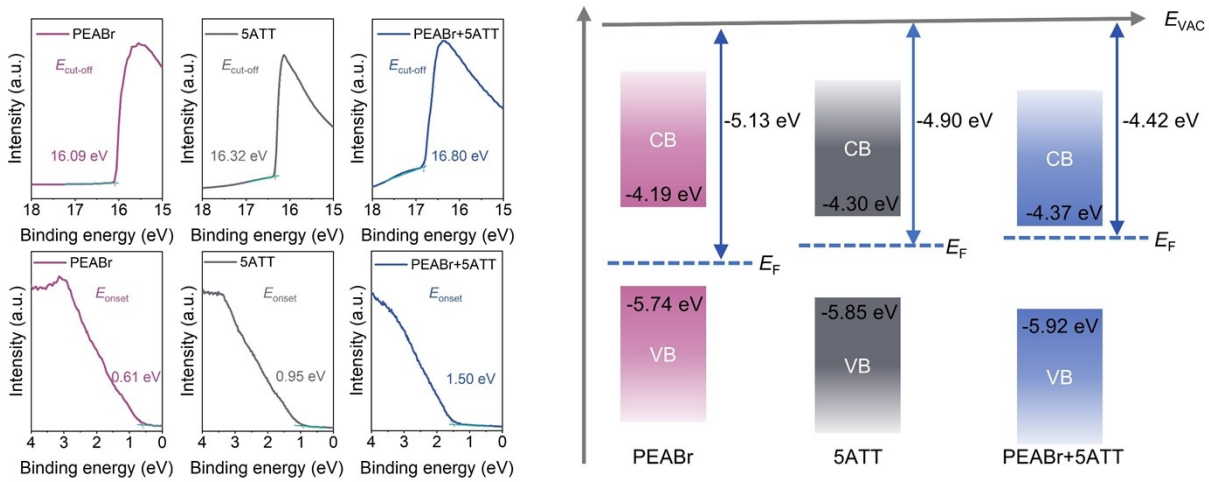

Fig. S19. UPS spectra and schematic energy level diagrams of 5ATT-, PEABr- and PEABr+5ATT-treated perovskite films.

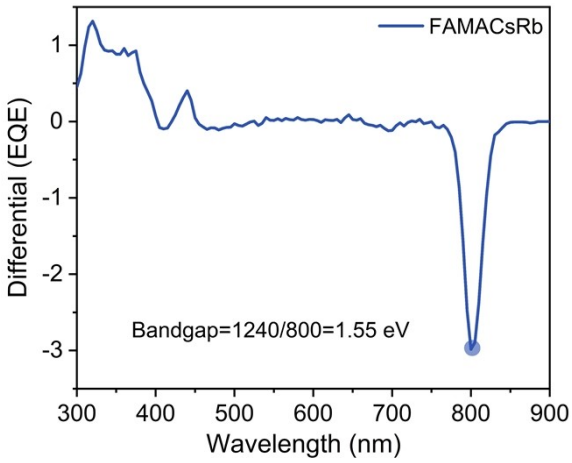

Fig. S20. The calculated bandgap of FAMACsRb perovskite based on the EQE spectrum.

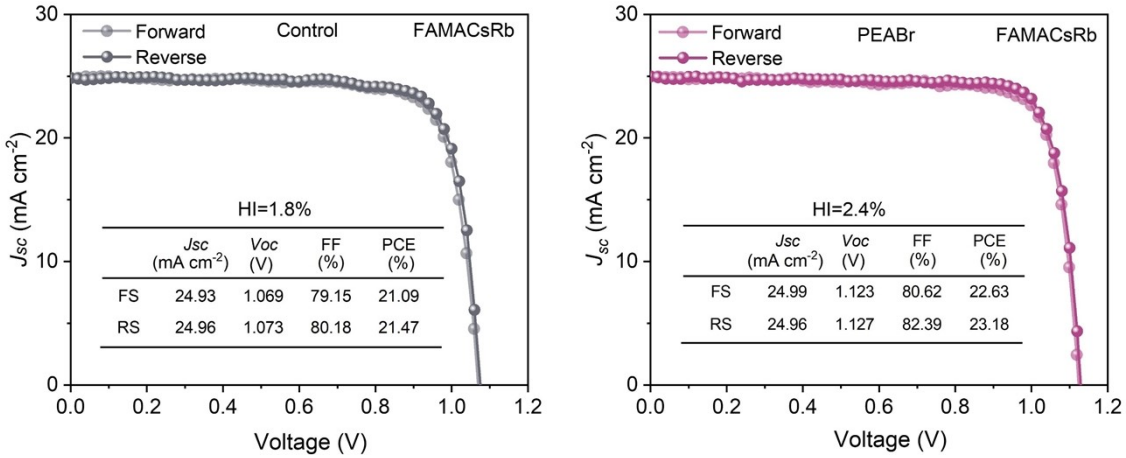

Fig. S21. PCEs of the control and PEABr-treated devices based on FAMACsRb perovskite.

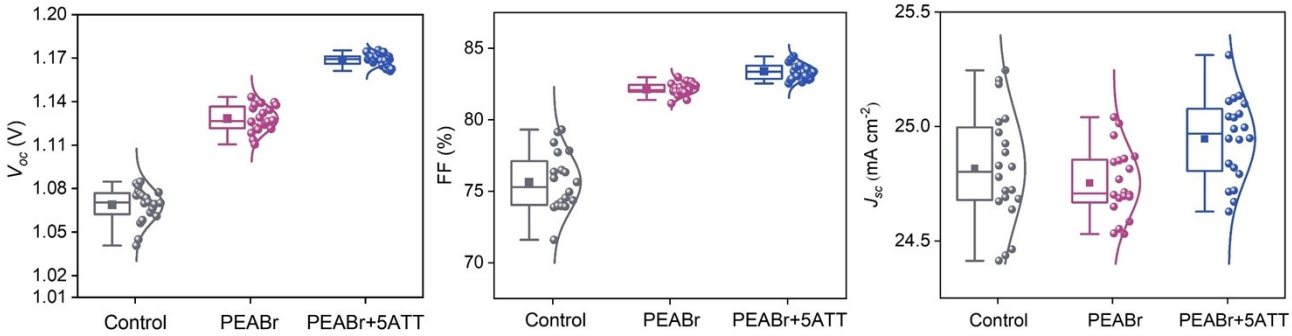

Fig. S22. The statistical V_{oc}, FF and J_{sc} of the control, PEABr- and PEABr+5ATT-treated devices.

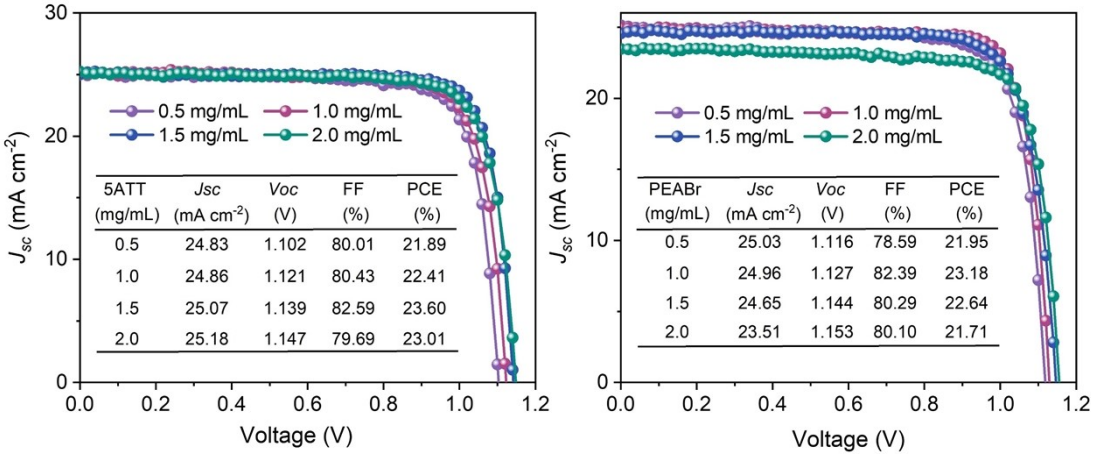

Fig. S23. The best PCEs of devices only using 5ATT (or PEABr) with different concentrations.

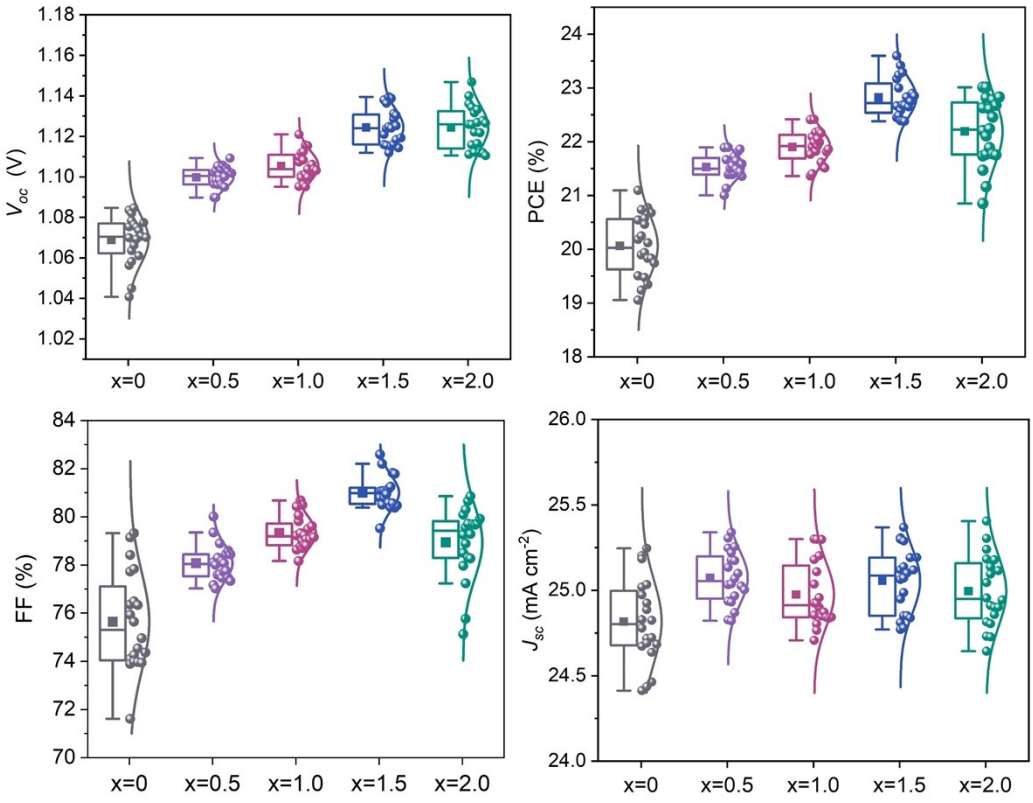

Fig. S24. The statistical V_{oc}, PCE, FF and J_{sc} of devices treated by 5ATT with different concentrations.

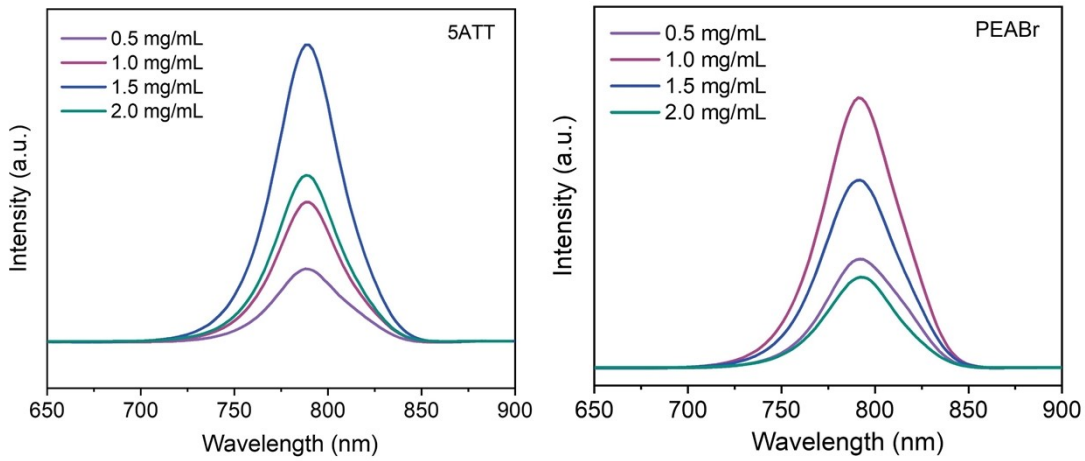

Fig. S25. PL results of only 5ATT- and PEABr-treated perovskite films based on passivation agents with different concentrations.

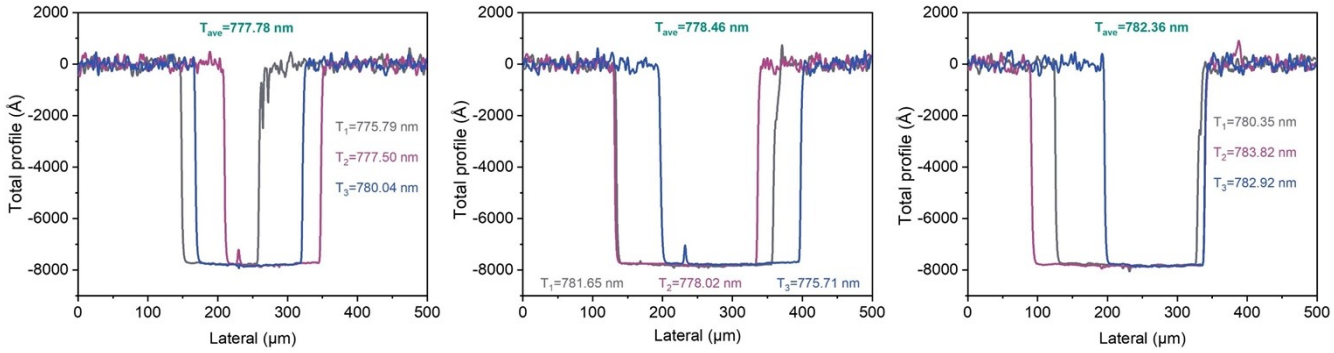

Fig. S26. The thicknesses of the control, PEABr- and PEABr+5ATT-treated perovskite films for N_{trap} calculations.

Chengdu Institute of Product Quality Inspection Co., Ltd.
National Photovoltaic Product Quality Inspection &Testing Center
TEST REPORT

Test Report No.AGXB124W00679 Page 1 of 3

Product Name	PSC-19.7	Trade Mark	/
Manufacture Date	/	Model /Type	Perovskite solar cells
Sample No.	AGXB124W00679	Sample Grade	/
Sample Quantity	One piece	Sample State	/
Delivery Date	20/11/2024	Sample Delivered personnel	Wenwu Zhou
Commission unit	Nanjing university	Manufacturer	Nanjing university
Commission unit address	163 Xianlin Road, Qixia District, Nanjing,Jiangsu Province	Manufacturer Address	163 Xianlin Road, Qixia District, Nanjing,Jiangsu Province
Commission unit Zip code	210023	Manufacturer Zip code	/
Commission unit Tel.	/	Manufacturer Tel.	/
Center Address	No. 355, 2nd Tengfei Road, Southwest Airport Economic Development Zone, Chengdu, Sichuan, P. R. China.	Measurement Date	20/11/2024
Methods	IEC 60904-1:2020 Photovoltaic devices-Part 1: Measurement of Photovoltaic Current-Voltage Characteristics.		
Test conclusion	This column blank.		
Remarks	Mask area: 0.06034cm².		

(Special chapter for test report)

Issue Date: 16/12/2024

检验检测专用章 检验检测专用章

Approved by **Reviewed by** **Measured by**

Fig. S27-1. Certified PCE of the best device based on FAMACs perovskite components by National Photovoltaic Product Quality Inspection & Testing Center.

Chengdu Institute of Product Quality Inspection Co., Ltd.
National Photovoltaic Product Quality Inspection &Testing Center
TEST REPORT

Test Report No.AGXB124W00679 Page 2 of 3

Test Results（Forward scanning）:

No.	Test item(s)	Unit	Results
1	Current-voltage characteristics measurement	---	---
1.1	Open-circuit voltage, V_{oc}	V	1.183
1.2	Short-circuit current, I_{sc}	mA	1.542
1.3	Maximum-power, P_{max}	mW	1.512
1.4	Maximum-power voltage, $V_{p\text{-}max}$	V	1.020
1.5	Maximum-power current, $I_{p\text{-}max}$	mA	1.482
1.6	Fill factor, FF	%	82.87
1.7	Conversion efficiency, η	%	25.06

Current-voltage characteristics under STC

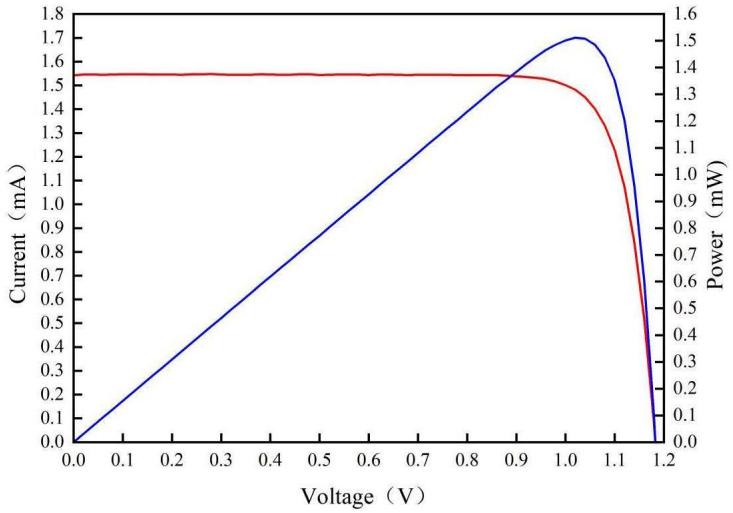

Remark: Sample was tested under the irradiation with a steady-state class calibrated AAA solar simulator (AM1.5-G 1000.0 W/m² basted on mono-Si reference cell) at 25±1 °C. Designated area defined by thin metal aperture mask.
The measuring uncertainty : U_{rel}(Pmax)=2.85%(k=2); U_{rel}(Isc)=2.69%(k=2); U_{rel}(Voc)=1.57%(k=2).

Fig. S27-2. Certified PCE of the best device based on FAMACs perovskite components by National Photovoltaic Product Quality Inspection & Testing Center.

Chengdu Institute of Product Quality Inspection Co., Ltd.
National Photovoltaic Product Quality Inspection &Testing Center
TEST REPORT

Test Report No. AGXB124W00679 Page 3 of 3

Test Results（Reverse scanning）:

No.	Test item(s)	Unit	Results
2	Current-voltage characteristics measurement	---	---
2.1	Open-circuit voltage, V_{OC}	V	1.184
2.2	Short-circuit current, I_{SC}	mA	1.546
2.3	Maximum-power, P_{max}	mW	1.535
2.4	Maximum-power voltage, $V_{p\text{-}max}$	V	1.040
2.5	Maximum-power current, $I_{p\text{-}max}$	mA	1.476
2.6	Fill factor, FF	%	83.86
2.7	Conversion efficiency, η	%	25.44

Current-voltage characteristics under STC

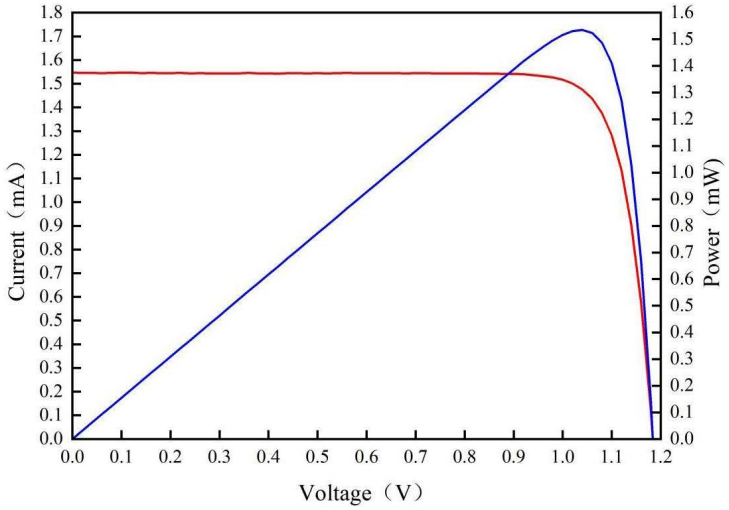

Remark: Sample was tested under the irradiation with a steady-state class calibrated AAA solar simulator (AM1.5-G 1000.0 W/m² basted on mono-Si reference cell) at 25±1 °C. Designated area defined by thin metal aperture mask.
The measuring uncertainty : U_{rel}(Pmax)=2.85%(k=2); U_{rel}(Isc)=2.69%(k=2); U_{rel}(Voc)=1.57%(k=2).

————Blank————

Fig. S27-3. Certified PCE of the best device based on FAMACs perovskite components by National Photovoltaic Product Quality Inspection & Testing Center.

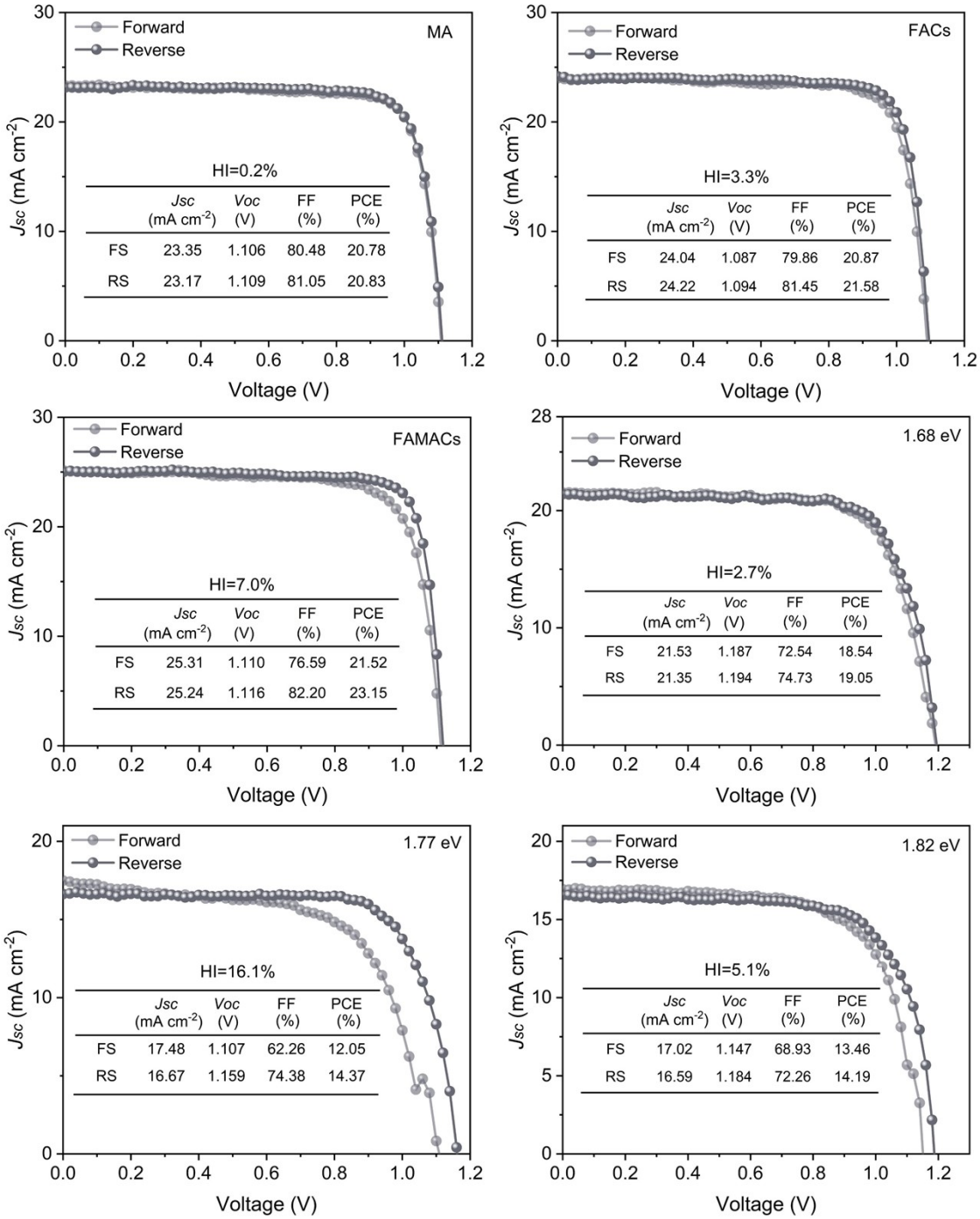

Fig. S28. The best PCEs of control devices based on MA, FACs, FAMACs, 1.68, 1.77 and 1.82 eV perovskites.

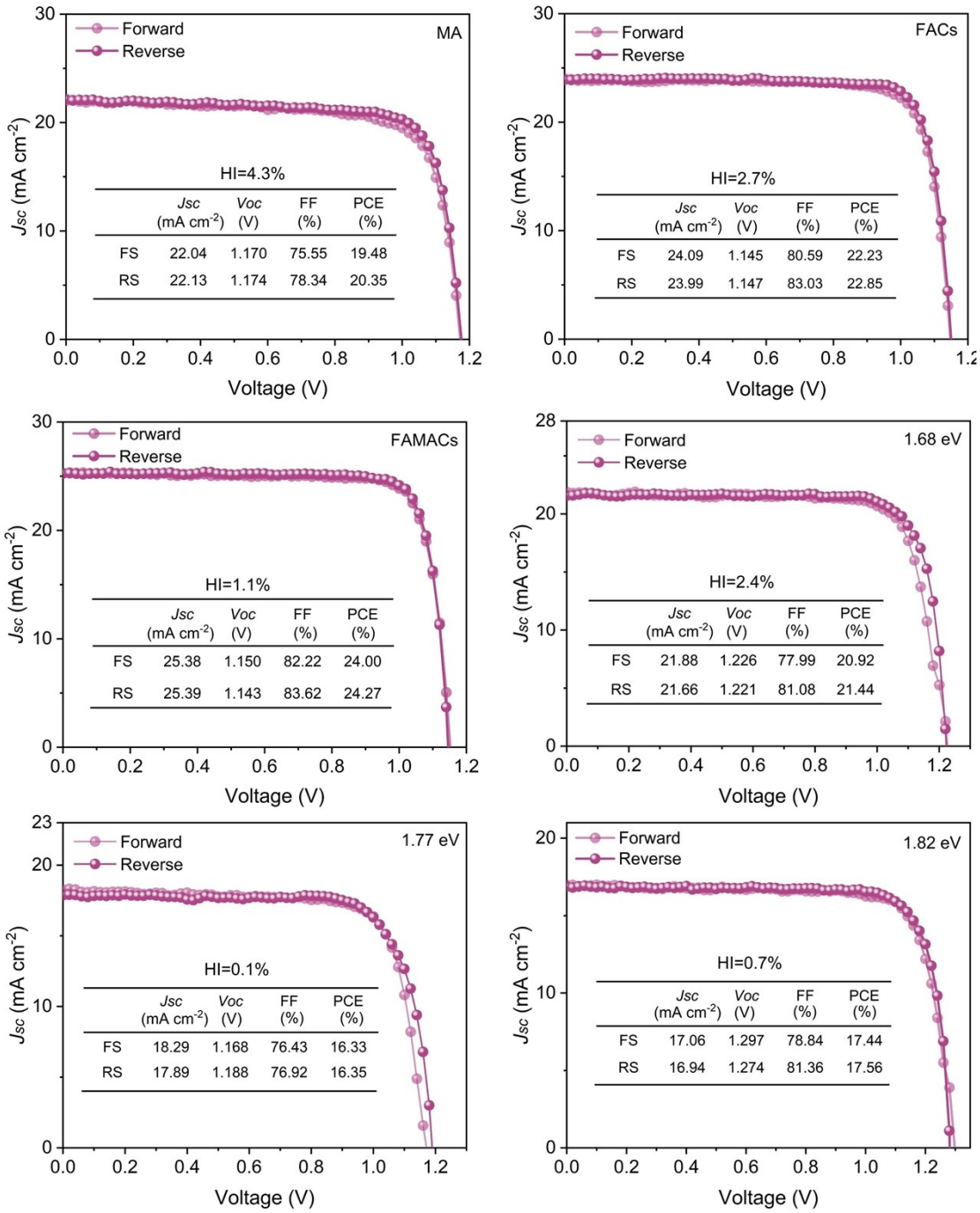

Fig. S29. The best PCEs of PEABr-treated devices based on MA, FACs, FAMACs, 1.68, 1.77 and 1.82 eV perovskites.

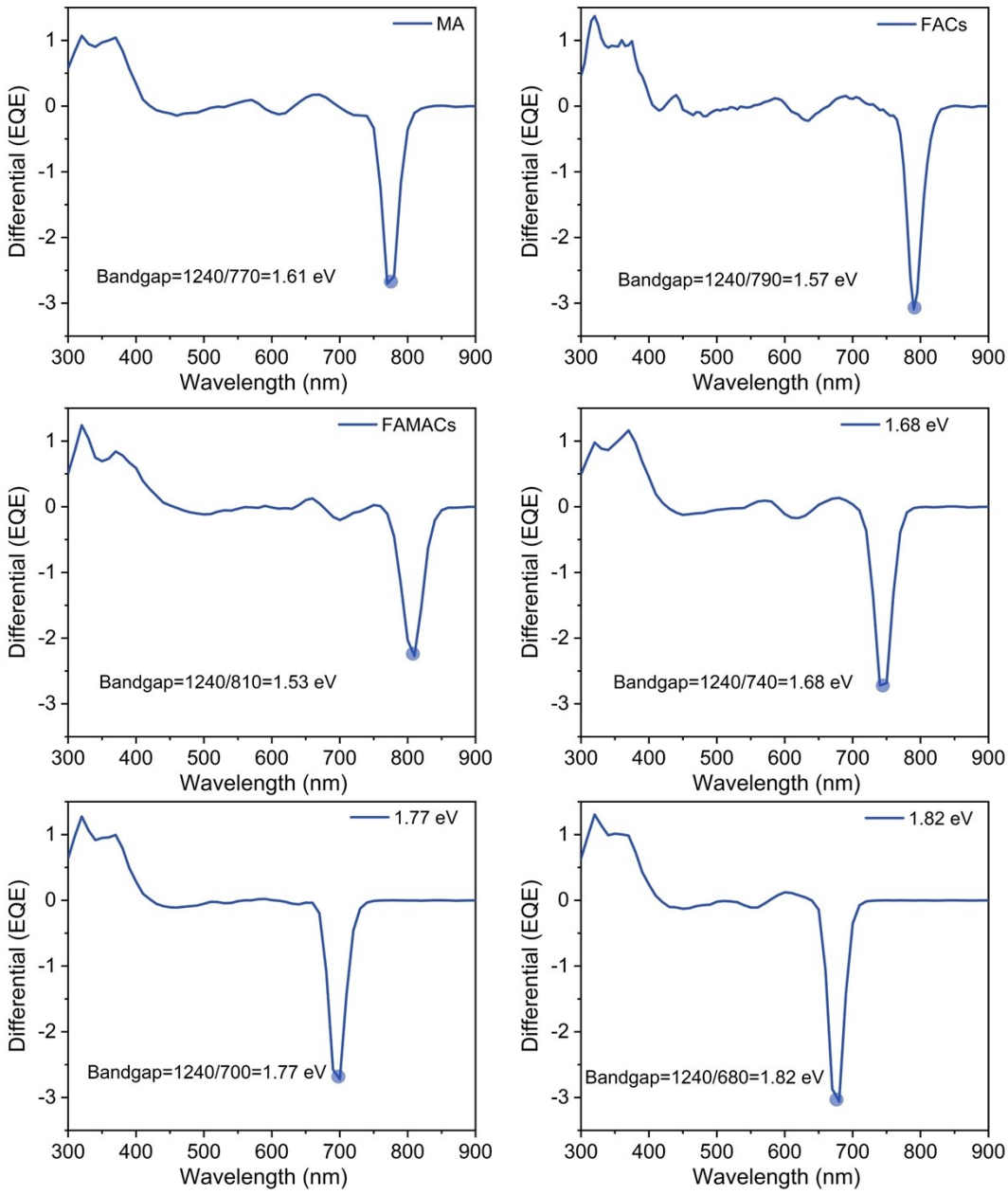

Fig. S30. The calculated bandgaps for MA, FACs, FAMACs, 1.68, 1.77 and 1.82 eV PSCs.

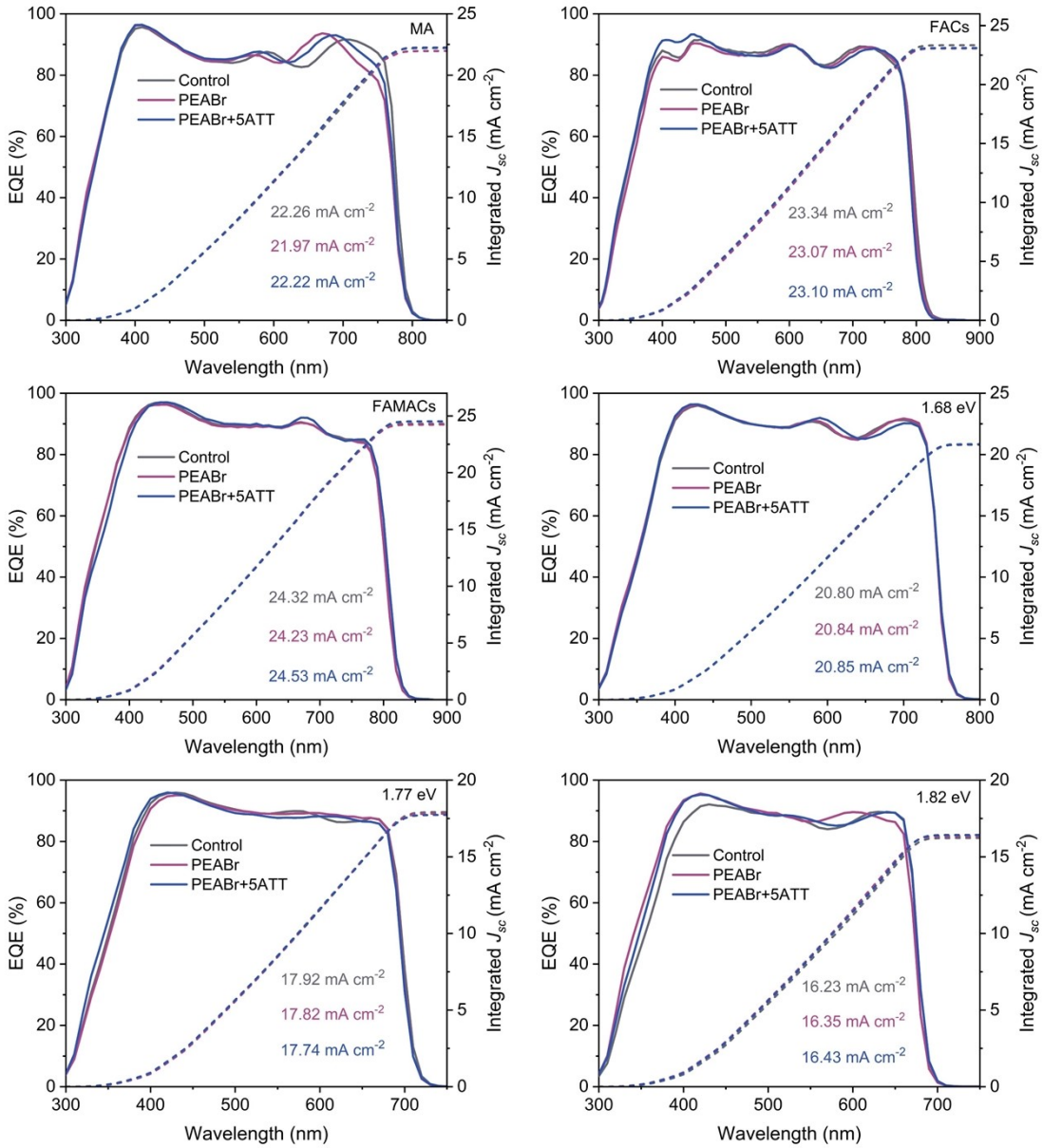

Fig. S31. The EQE spectra and integrated current densities of the control, PEABr- and PEABr+5ATT-treated devices.

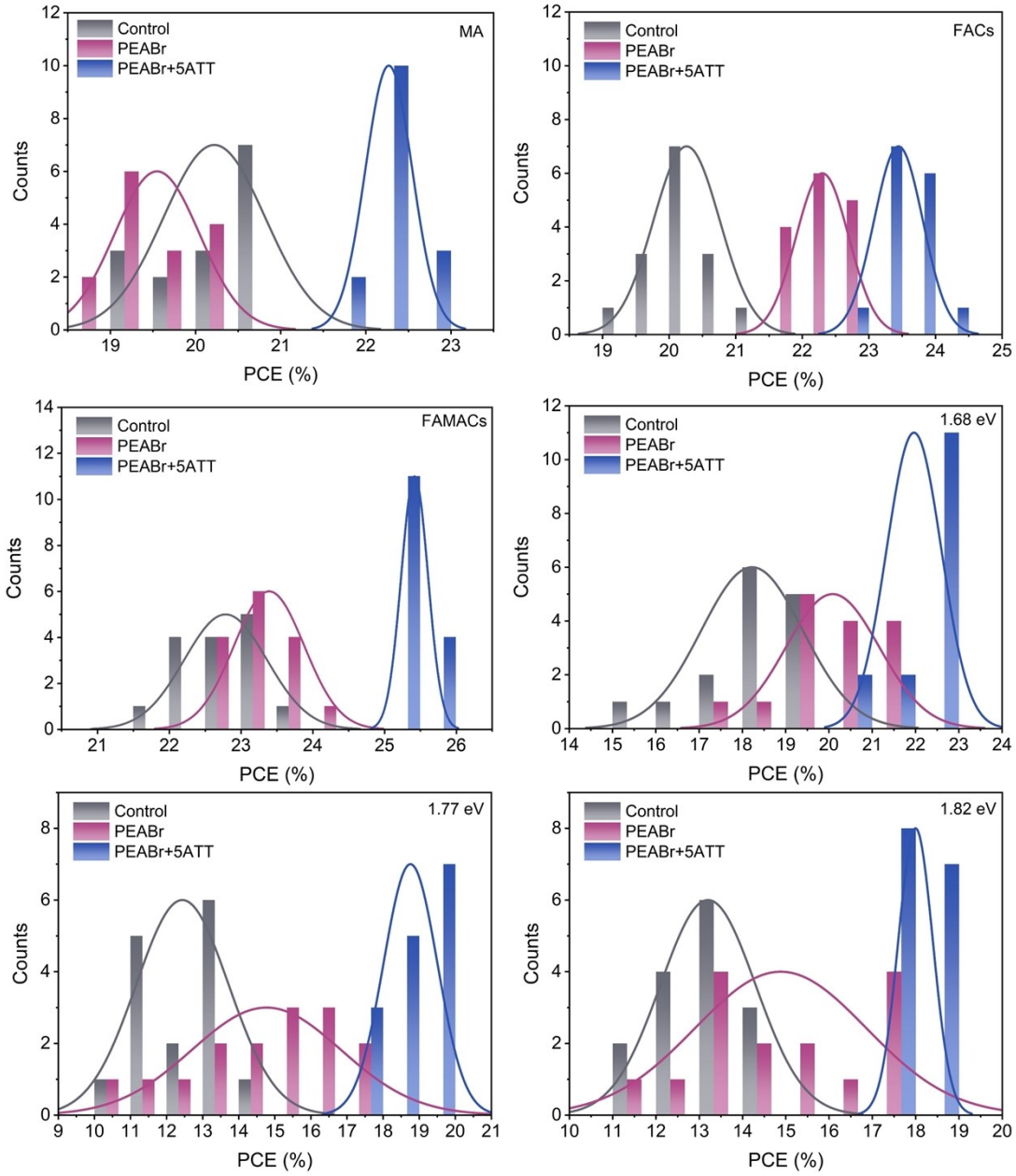

Fig. S32. The statistical PCEs of the control, PEABr- and PEABr+5ATT-treated devices (15 individual devices for each) with different components and various bandgaps.

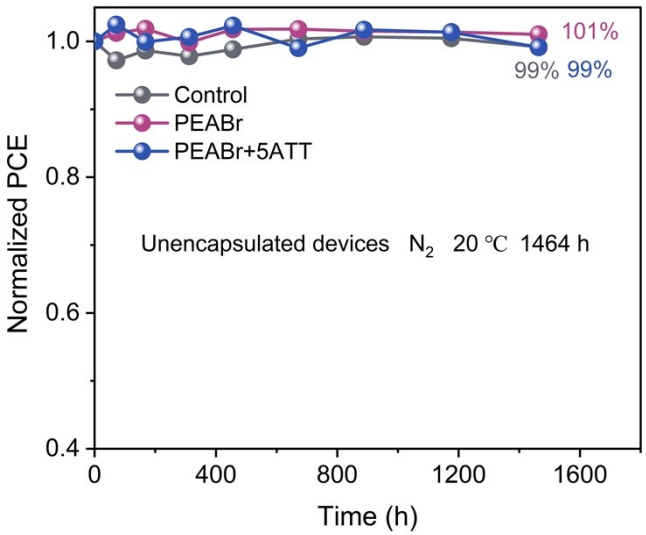

Fig. S33. The stability of the unencapsulated devices after storing at the N_2 atmosphere for 1464 hours.

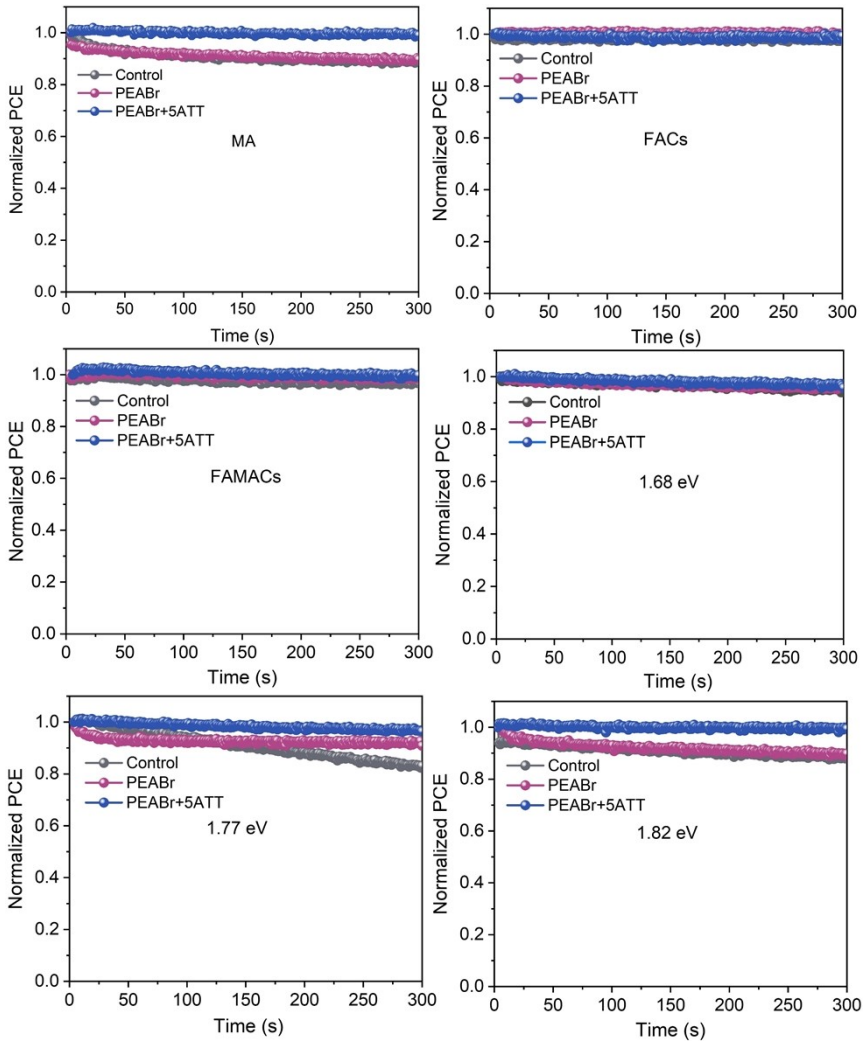

Fig. S34. The MPP tracking tests of MA, FACs, FAMACs, 1.68, 1.77 and 1.82 eV devices treated with passivating agents in N_2 atmosphere at 25 ℃. (1.68, 1.77 and 1.82 eV devices were based on NiO_x-stabilized SAM, while other devices were measured without NiO_x).

Table S1. The fitted parameters of carrier lifetimes of the control, PEABr- and PEABr+5ATT-treated perovskite films.

Films	A_1	τ_1 (ns)	A_2	τ_2 (ns)	τ_{avg} (ns)
Control	0.657	12.6	0.343	465.9	168.1
PEABr	0.583	189.2	0.417	2610.3	1199.4
PEABr+5ATT	0.603	111.0	0.397	3270.2	1366.4

Table S2. The related calculation results of QFLS based on the PLQY data.

Films	PLQY (%)	J_G (A m^{-2})	$J_{0,\,rad}$ (A m^{-2})	$QFLS_{rad}$ (eV)	QFLS (eV)
Control	4.64	238.9	1.52×10^{-19}	1.263	1.183
Control/$PC_{61}BM$	0.09				1.081
PEABr	5.52	239.2	1.31×10^{-19}	1.267	1.192
PEABr/$PC_{61}BM$	0.80				1.142
PEABr+5ATT	8.63	241.3	1.44×10^{-19}	1.264	1.201
PEABr+5ATT/$PC_{61}BM$	4.13				1.182

Table S3. Summary of the recent reported photovoltaic parameters of PSCs by interfacial engineering.

Perovskite components	Device architecture	PCE (%)	Ref.
$Cs_{0.05}FA_{0.80}MA_{0.15}Pb(I_{0.85}Br_{0.15})_3$ (1.63 eV)	FTO/c-TiO_2/m-TiO_2/ PVSK/**FABr**/Spiro-OMeTAD/Au	22.1	5
$Cs_{0.05}MA_{0.15}FA_{0.80}Pb(I_{0.95}Br_{0.05})_3$ (1.56 eV)		23.7	
$MAPbI_3$ (1.60 eV)		21.4	
$CsPbIBr_2$ (2.11 eV)	FTO/c-TiO_2/ PVSK/**BN**/Carbon	12.05	6
$CsPbI_2Br$ (1.90 eV)		14.14	
$FA_{0.92}MA_{0.08}PbI_3$ (1.55 eV)	FTO/SnO_2/PVSK/**BN**/ Spiro-OMeTAD/Au	23.37	
$MAPbI_3$	ITO/PTAA/PVSK/ **$FcTc_2$**/C60/BCP/Ag	21.40	7
$FAPbI_3$		22.60	
$(FA_{0.98}MA_{0.02})_{0.95}Cs_{0.05}Pb(I_{0.95}Br_{0.02})_3$		25.00	
$(FAPbI_3)_{0.98}(MAPbBr_3)_{0.02}$ (1.55 eV)	ITO/Me-4PACz/ SiO_x-np/PVSK/**AlO_x**/ C60/SnO_x/Ag	23.32	8
$Cs_{0.05}(FA_{0.90}MA_{0.10})_{0.95}(I_{0.80}Br_{0.20})_3$(1.65 eV)		20.10	
CsFA (1.7 eV)		19.00	
$Cs_{0.13}FA_{0.87}Pb(I_{0.9}Br_{0.1})_3$ (1.60 eV)	ITO/Me-4PACz/PVSK/ **AEAPTMS**/PCBM/BCP/Cr/Au	22.60	9
$Cs_{0.17}FA_{0.83}Pb(I_{0.77}Br_{0.23})_3$ (1.67 eV)		20.60	
$Cs_{0.15}FA_{0.85}Pb(I_{0.60}Br_{0.40})_3$ (1.77 eV)		18.70	
$Cs_{0.05}MA_{0.05}FA_{0.90}PbI_3$ (~1.5 eV)	FTO/Me-4PACz/PVSK/ **DMDP**/C60/BCP/Ag	26.4	10
$Cs_{0.05}MA_{0.25}FA_{0.7}Pb_{0.5}Sn_{0.5}I_3$ (~1.2 eV)		~20.5	
$Cs_{0.2}FA_{0.8}PbI_{1.9}Br_{1.1}$ (~1.8 eV)		~19.4	
$CsPbI_{2.25}Br_{0.75}$	ITO/SnO_2/SnO_x/PVSK/ **TDCA**/PDTDT/Au	16.72	11
$CsPbI_{1.5}Br_{1.5}$		12.71	
$CsPbIBr_2$		10.08	
$MAPbI_3$	FTO/SnO_2/PVSK/**TOAC**/ Spiro-OMeTAD/Au	21.24	12
$Cs_{0.05}(FAPbI_3)_{0.83}(MAPbBr_3)_{0.17}$		19.27	
$MAPbI_3$	ITO/SnO_2/PVSK/**nHA**/ Spiro-OMeTAD/Ag	21.03	13
CsFAMA		23.7	
$MAPbI_3$ (1.61 eV)	ITO/SAM/PVSK/**PEABr+ 5ATT**/$PC_{61}BM$/BCP/Ag	22.61	This work
$FA_{0.85}Cs_{0.15}Pb(I_{0.95}Br_{0.05})_3$ (1.57 eV)		24.01	
$FA_{0.85}MA_{0.1}Cs_{0.05}PbI_3$ (1.53 eV)		25.88	
$FA_{0.85}MA_{0.05}Cs_{0.05}Rb_{0.05}Pb(I_{0.95}Br_{0.05})_3$(1.55eV)		24.85	
$FA_{0.8}MA_{0.15}Cs_{0.05}Pb(I_{0.75}Br_{0.25})_3$ (1.68 eV)		22.57	
$FA_{0.8}Cs_{0.2}Pb(I_{0.6}Br_{0.4})_3$ (1.77 eV)		19.61	
$FA_{0.8}MA_{0.1}Cs_{0.1}Pb(I_{0.5}Br_{0.5})_3$ (1.82 eV)		18.68	

References

1 H. Luo, X. Zheng, W. Kong, Z. Liu, H. Li, J. Wen, R. Xia, H. Sun, P. Wu, Y. Wang, Y. Mo, X. Luo, Z. Huang, J. Hong, Z. Chu, X. Zhang, G. Yang, Y. Chen, Z. Feng, J. Gao and H. Tan, *ACS Energy Lett.*, 2023, **8**, 4993-5002.

2 W. Zhou, S. Tai, Y. Li, H. Fu and Q. Zheng, *Adv. Funct. Mater.,* 2024, **34**, 2407897.

3 A. I. A. Soliman, Y. Zhang, L. Zhang, H. Wu, S. Shan, Y. Zhou, C. Xu, W. Fu and H. Chen, *Adv. Funct. Mater.*, 2024, 2412886.

4 T. Yang, L. Gao, J. Lu, C. Ma, Y. Du, P. Wang, Z. Ding, S. Wang, P. Xu, D. Liu, H. Li, X. Chang, J. Fang, W. Tian, Y. Yang, S. F. Liu and K. Zhao, *Nat. Commun.,* 2023, **14**, 839.

5 Y. Li, W. Xu, N. Mussakhanuly, Y. Cho, J. Bing, J. Zheng, S. Tang, Y. Liu, G. Shi, Z. Liu, Q. Zhang, J. R. Durrant, W. Ma, A. W. Y. Ho-Baillie, S. Huang, *Adv. Mater.,* 2022, **34**, 2106280.

6 Q. Guo, J. Duan, J. Zhang, Q. Zhang, Y. Duan, X. Yang, B. He, Y. Zhao, Q. Tang, *Adv. Mater.*, 2022, **34**, 2202301.

7 Z. Li, B. Li, X. Wu, S. A. Sheppard, S. Zhang, D. Gao, N. J. Long, Z. Zhu, *Science,* 2022, **376**, 416.

8 K. Artuk, D. Turkay, M. D. Mensi, J. A. Steele, D. A. Jacobs, M. Othman, X. Yu Chin, S. J. Moon, A. N. Tiwari, A. Hessler-Wyser, Q. Jeangros, C. Ballif, C. M. Wolff, *Adv. Mater.*, 2024, **36**, 2311745.

9 Y. H. Lin, Vikram, F. Yang, X. L. Cao, A. Dasgupta, R. D. J. Oliver, A. M. Ulatowski, M. M. McCarthy, X. Shen, Q. Yuan, M. G. Christoforo, F. S. Y. Yeung, M. B. Johnston, N. K. Noel, L. M. Herz, M. S. Islam, H. J. Snaith, *Science,* 2024, **384**, 767.

10 C. Liu, Y. Yang, H. Chen, J. Xu, A. Liu, A. S. R. Bati, H. Zhu, L. Grater, S. S. Hadke, C. Huang, V. K. Sangwan, T. Cai, D. Shin, L. X. Chen, M. C. Hersam, C. A. Mirkin, B. Chen, M. G. Kanatzidis, E. H. Sargent, *Science,* 2023, **382**, 810.

11 Z. Guo, S. Zhao, N. Shibayama, A. Kumar Jena, I. Takei, T. Miyasaka, *Adv. Funct. Mater.,* 2022, **32**, 2207554.

12 S. Y. Abate, Q. Zhang, Y. Qi, J. Nash, K. Gollinger, X. Zhu, F. Han, N. Pradhan, Q. Dai, *ACS Appl. Mater. Interfaces.,* 2022, **14**, 28044.

13 M. Wang, H. Sun, L. Meng, M. Wang, L. Li, *Adv. Mater.,* 2022, **34**, 2200041.